ISPRS Journal of Photogrammetry and Remote Sensing 96 (2014) 28–37

Contents lists available at ScienceDirect

ISPRS Journal of Photogrammetry and Remote Sensing

journal homepage: www.elsevier.com/locate/isprsjprs

An automated approach to vertical road characterisation using mobile LiDAR systems: Longitudinal profiles and cross-sections

Alberto Holgado-Barco [a], Diego Gonzalez-Aguilera [a,*], Pedro Arias-Sanchez [b], Joaquín Martinez-Sanchez [b]

[a] Department of Cartographic and Land Engineering, University of Salamanca, Higher Polytechnic School of Avila, Hornos Caleros 50, 05003 Avila, Spain
[b] Department of Natural Resources & Environmental Engineering, University of Vigo, School of Mining Engineering, Maxwell s/n, 36310 Vigo, Spain

ARTICLE INFO

Article history:
Received 9 February 2014
Received in revised form 28 June 2014
Accepted 30 June 2014
Available online 24 July 2014

Keywords:
Mobile mapping system
Mobile LiDAR system
Geospatial information
Laser surveying
Road maintenance
Road inventories
Vertical alignment
Segmentation
Filtering
Parameterisation
Feature extraction

ABSTRACT

The characterisation the vertical profiles and cross-sections of roads is important for the verification of proper construction and road safety assessment. The goal of this paper is the extraction of geometric parameters through the automatic processing of mobile LiDAR system (MLS) point clouds. Massive and complex datasets provided by the MLS are processed using a hierarchical strategy that includes segmentation, principal component analysis (PCA)-based orthogonal regression, filtering and parameter extraction procedures. Best-fit geometric parameters act as a vertical road model for both linear parameters (slope and vertical curves) and cross-sections (superelevations). The proposed automatic processing approach gives satisfactory results for the analysed scenario.

1. Introduction

The availability of a detailed digital cartography for road geometry is of great importance when working with topographic applications centred on road characterisation for engineering purposes such as route modifications (i.e., lane additions). In the same way, the analysis of digital road maps can enhance road-safety verification, the identification of potentially dangerous points or black-spot localisation and the influence of road conditions on accident forensics (Gomes, 2013).

The literature contains numerous examples of the use of road planning for road-safety-based modification. Sentouh et al. (2006) conducted a road speed analysis for accident prevention. In this work, the vehicle, driver and infrastructure were modelled to obtain the maximal speed in curve, and the infrastructure characteristics included both the horizontal and vertical geometric information. Taylor et al. (2007) proposed a speed model based on artificial neural networks for road-safety analysis. The inputs to the model included horizontal and vertical road alignment. The European project SAFESTAR-Safety Standards for Road Design and Redesign (Institute for Road Safety Research, 2002) attached great importance to the knowledge of road layouts, assessing the safety of road infrastructure during road planning and design.

Applying mobile LiDAR systems (MLS) to road surveying is straightforward and allows for a wide range of possible applications. Gräfe (2008) presented a capture system that allows a surface model to be obtained for the planning and design of roads. Ai and Tsai (2012) presented and assessed an automated method for traffic sign detection using LiDAR point clouds. El-Halawany and Lichti (2011) proposed a pipeline for road pole detection through MLS processing. This method is based on the eigenvalue analysis of the covariance matrix in a local neighbourhood. Yang et al. (2012) presented an approach to automated road-marking extraction based on a hierarchical segmentation methodology using point-intensity and point-height thresholds, followed by a knowledge-based extraction. Wang et al. (2013) focused on obtaining data of interest on excavation volume extraction for road construction through MLS data processing.

The automatic extraction of road layouts from MLS makes possible the availability of detailed digital road maps that contain precise information on widely used geometric parameters, both

* Corresponding author.
E-mail address: daguilera@usal.es (D. Gonzalez-Aguilera).

http://dx.doi.org/10.1016/j.isprsjprs.2014.06.017
0924-2716/

horizontal (straight lines, circular curves and clothoids) and vertical (slope, vertical curves and superelevations). A number of authors recently employed mobile mapping systems (MMS) to derive precise information on horizontal and vertical road parameters. Karamanou et al. (2010) proposed the use of a survey based on the geodetic positioning of a suitably equipped vehicle moving along the road in a two-way journey. The acquired data were used to extract the road's centreline. The parameters of the road's horizontal and vertical features were then estimated based on a least squares adjustment of the characteristic curves. Di Mascio et al. (2012) presented a procedure to determine the geometry of horizontal and vertical road alignment using a global navigation satellite system's (GNSS) dynamic measurements. Two datasets were logged for a single carriageway, one for each traffic direction, and the centreline was estimated as the middle point between both trajectories. Another algorithm was then applied to recognise the horizontal and vertical road elements through least squares optimisation. Gikas and Stratakos (2012) proposed a method, based on the trajectory captured by a GNSS, for deriving curvature diagrams and analysing the horizontal geometric elements of a road/railway. Lakakis et al. (2013) developed a low-cost system supported only by two GNSS sensors that could obtain the vertical alignment of a road. Again, a two-way journey was required to survey the road. Tsai et al. (2013) presented a method based on MLS acquisition, but focused only on the computation of superelevations. More recently, (Holgado-Barco et al., 2014) proposed a method for the extraction of horizontal geometric road alignments based on MLS processing. This method was followed by an assessment of the obtained road alignment using official ground-truth data.

One of the main disadvantages of these studies is that results analysis and comparison are usually non-quantitative due to the lack of a comparative ground-truth. Among the studies that provide a vertical road analysis, their analysis is usually limited to the vehicle lane, extracting cross-section slopes with no linear slope extraction. In addition, those approaches based only on GNSS measurements require a two-way journey, whereas the studies performed with a MLS do not provide a complete vertical alignment analysis. Within this context, this paper presents a workflow for the automatic extraction of geometric vertical road parameters through MLS data processing, distinguishing linear (i.e., slopes and vertical curves) and cross-sectional (i.e., superelevations) parameters. Finally, the parameters are created according to Spanish road regulations and their absolute and relative errors are estimated to evaluate the method's accuracy.

In Section 2, the materials and methods used in the study are explained, emphasising segmentation, principal component analysis (PCA)-based orthogonal regression, setup and filtering. Section 3 provides the experimental results obtained using a dataset, while the last section describes the conclusions drawn from this work and future research suggestions.

2. Materials and methods

2.1. Capture system: Optech LYNX MMS

The capture system used in this work is a LYNX Mobile Mapper manufactured by Optech (Optech, 2013) (see Fig. 1). This system is composed of two LiDAR sensors, four RGB cameras, and an Applanix POS LV 520 IMU. The system is configured to take 500,000 points per second with a scan frequency of 200 Hz. The maximum range of the sensors is 200 m, with a precision of 8 mm (one sigma) and permission to obtain up to 4 echoes of the signal and the intensity reflected by the objects at a 1550 nm wavelength (Puente et al., 2012). These and other characteristics are listed in Table 1.

Fig. 1. The Optech LYNX Mobile Mapper.

Table 1
Technical characteristics of Optech LYNX Mobile Mapper.

Technical features	LYNX Mobile Mapper
X, *Y* position	0.020 m
Z position	0.050 m
Roll and pitch	0.005°
True heading	0.015°
Measuring principle	Time of flight (TOF)
Maximum range	200 m
Range precision	8 mm, 1σ
Range accuracy	±10 mm, (1σ)
Laser measurement rate	75–500 kHz
Measurement per laser pulse	Up to 4 simultaneous
Scan frequency	80–200 Hz
Laser wavelength	1550 nm (near infrared)
Scanner field of view	360°
Operating temperature	10°–40 °C
Angular resolution	0.001°

2.2. Methodology overview

The proposed methodology is carried out in four steps (see Fig. 2). The first step is data capture through MLS, and the following processing steps are focused on segmentation, plane adjustment and point cloud parameter extraction. Specifically, the goal of the segmentation is to simplify the point cloud to extract a road platform and provide cross-sections along with the trajectory. Next, a process for creating a best-fit plane is performed using PCA. This plane adjustment of the road allows the geometric parameters of the vertical and cross-sections to be extracted, accounting for slope and superelevation diagrams. More precisely, these geometric parameters are obtained from the eigenvalues and eigenvectors computed with the PCA. Due to the presence of gross and accidental errors in the input data and the parameter extraction, data filtering and processing are needed. A prototype of the process is fully developed in MatLab, due mainly to its ease of use in testing algorithms and obtaining research results, the goal being to extrapolate the developed approach to a powerful point cloud library (PCL) and an open source C++ library. The main advantage of using PCL is that many of its functions are parallelised and thus improve the software's performance.

2.3. Point cloud segmentation

The input point cloud provided by the MLS is segmented in a two-step approach. The first segmentation phase is achieved by setting angular thresholds in a road function with user interaction

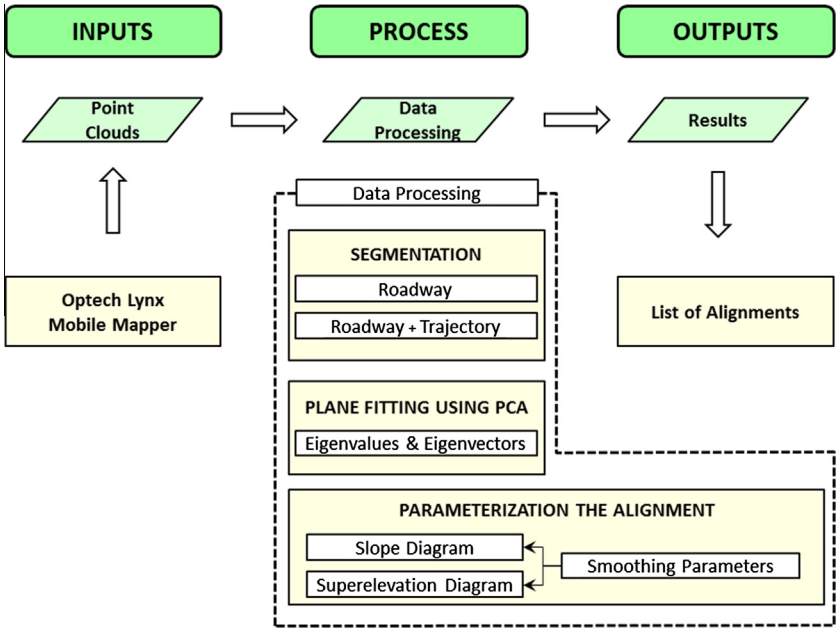

Fig. 2. Workflow of the developed processing.

and the second phase based on the generation of the road's cross-sections.

The goal of the first segmentation phase is to set the angular thresholds and produce a rough calculation of the road platform. Noting that the laser heads consist of a laser distance meter that is deflected by a mirror to create 2D sections, we can define a polar local coordinate system centred in each laser (see Fig. 3). During the first segmentation phase, this local coordinate system is used to set the minimum and maximum values for the angular coordinate. In our case, for highways that obey the Spanish Road Rules, minimum and maximum values of 196° and 336° are derived when the MLS is travelling in the right lane. These values should be refined for different road types or rules.

Once the platform segmentation is completed, the next step consists of generating 1 m long cross-sections, with respect to the MLS travelling route, that contain approximately 8800 points. The cross-sections are obtained using the trajectory of the MLS as a reference based on the *XY* coordinates and the azimuth of 1 m spaced points. Two anchor points are computed from these reference points on the trajectory using Eq. (1):

$$\begin{aligned} x &= x_0 + r \cdot \cos\theta \\ y &= y_0 + r \cdot \sin\theta \end{aligned} \tag{1}$$

where x and y are the coordinates of the anchor points, x_0 and y_0 are the coordinates of the reference point on the trajectory, r is the distance between the trajectory and the road platform's extreme points and θ is the direction orthogonal to the trajectory. These auxiliary anchor points are used for segmentation (see Fig. 4).

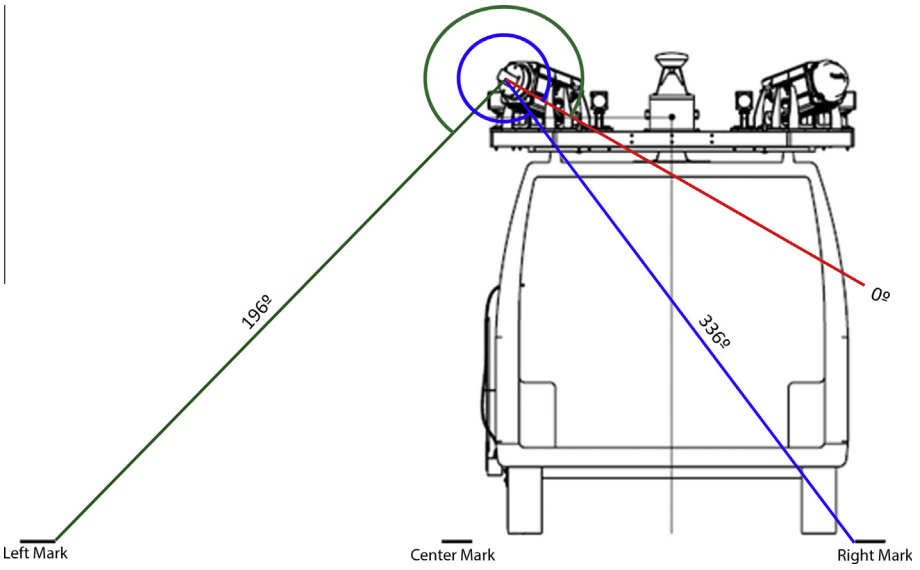

Fig. 3. Angular segmentation angles for road platform determination.

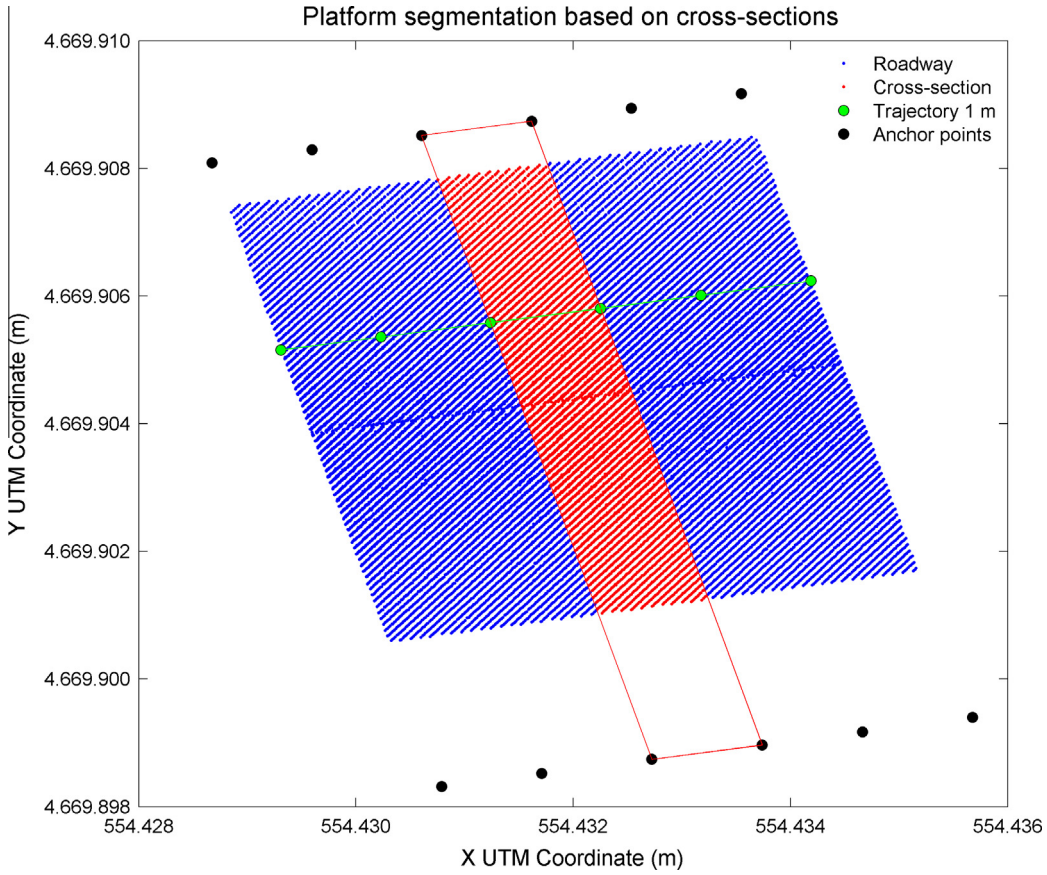

Fig. 4. Platform segmentation based on 1 m-long sections. Selected points are highlighted in red. The width of the cross-sections equals the width of the road platform, which is 7 m in our case. (For interpretation of the references to colour in this figure legend, the reader is referred to the web version of this article.)

2.4. Slope and superelevation computation using PCA

After the angular and cross-section segmentation is applied, selected points belonging to rectangular regions between the anchor points are processed for plane adjustment using PCA. The plane adjustment, based on a covariance matrix, allows for computation of the slope and superelevation (Belton and Lichti, 2006; Pauly et al., 2002) using the eigenvalues and eigenvectors corresponding to each cross-section.

By using PCA, a linear transformation to a new coordinate system is achieved to reduce the dimensionality of the original dataset (Jolliffe, 2002). The basis vectors of this new coordinate system are given by the principal components in the data. The first step in the PCA is to obtain the covariance matrix, which is described by Eq. (2):

$$\Sigma = COV(X) = \begin{bmatrix} \sigma_x^2 & \sigma_{xy} & \sigma_{xz} \\ \sigma_{xy} & \sigma_y^2 & \sigma_{yz} \\ \sigma_{xz} & \sigma_{yz} & \sigma_z^2 \end{bmatrix} \quad (2)$$

where $\sigma_x{}^2$ and σ_{xy} represent the variance and covariance, respectively:

$$\sigma_x^2 = \mathrm{var}(x) = E(x^2) - E(x)^2 = \frac{1}{k}\sum_{i=1}^{k}(x_i - \bar{x})^2 \quad (3)$$

$$\sigma_{xy} = \mathrm{cov}(x,y) = E(xy) - E(x)E(y) = \frac{1}{k}\sum_{i=1}^{k}(x_i - \bar{x})(y_i - \bar{y}) \quad (4)$$

x_i, y_i and z_i are the coordinates of the segmented points, k is the number of points in the original dataset and $\bar{x}, \bar{y}$ are the data centroid coordinates.

The next step involves the calculation of the eigenvalues and eigenvectors of this matrix. The eigenvalues can be derived from Eq. (5):

$$|\Sigma - \lambda \cdot I| = 0 \quad (5)$$

Given that Σ is a symmetric matrix, its corresponding eigenvectors form a basis of the vector space and obey Eq. (6):

$$\Sigma \cdot v = \lambda \cdot v \quad (6)$$

where Σ is the covariance matrix and v are the eigenvectors ($v_0 v_1 v_2$) associated with the eigenvalues λ ($\lambda_0 \lambda_1 \lambda_2$). The transformation from the original vector basis to this new basis is the linear transformation that reduces the dataset dimensionality.

Three eigenvalues and eigenvectors of the matrix are obtained using PCA. These values contain geometric information that is suitable for geometric characterisation of the road's vertical profile. Specifically, the eigenvector, v_0, corresponding to the smallest eigenvalue, λ_0, contains information about the adjusted normal plane, while the eigenvalues λ_1 and λ_2 and the corresponding eigenvectors v_1 and v_2 contain information about the slope (longitudinal) and superelevation (transversal). Fig. 5 shows the correspondence between the eigenvectors and eigenvalues and the road's geometric parameters. In the end, the percentage slope and superelevation are computed using Eq. (7) as a function of the corresponding eigenvector:

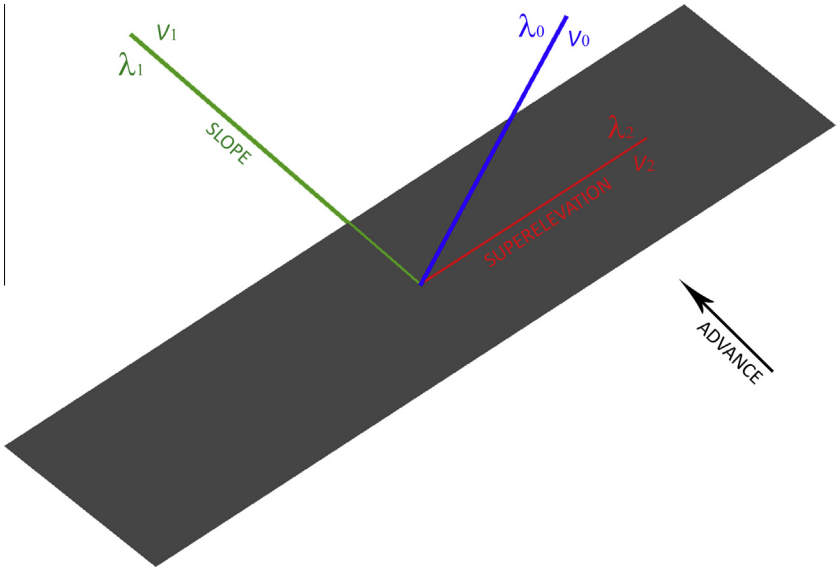

Fig. 5. Drawing showing the correspondence between PCA-based eigenvalues and eigenvectors with vertical geometric parameters of the road.

$$\text{Inclination } (\%) = \frac{v_z}{\sqrt{v_x^2 + v_y^2}} \cdot 100 \tag{7}$$

where v_x, v_y and v_z are the coordinates of each eigenvector.

2.5. Slope and superelevation smoothness filtering and geometric characterisation

Once the slope and superelevation are computed, a graphical parameterisation is implemented to improve the readability of the data. Graphical diagrams are commonly used as an accurate and detailed topographical representation of a road's vertical parameters.

Regarding the slope of the road, these vertical parameters are characterised in two ways, through vertical curves and slopes. In the first case, the slopes are drawn as straight lines that possess the same slope as the road, and the vertical agreement is modelled as a parabola. In the second case, the slope diagram consists of horizontal slope lines with straight vertical agreements. These two approaches are depicted in Fig. 6.

A relationship exists between a road's superelevation and its horizontal profile. Fig. 7 shows a graphical diagram of this relationship. The straight sections in the horizontal alignment correspond to normal crown zones in the superelevation diagram, whereas the circular arcs are related to the full superelevation that counteracts centrifuge. These sections are both depicted as horizontal lines in the superelevation diagram. The superelevation transition sections corresponding to clothoid arc alignments are modelled as lines with the slope in the superelevation diagram, adapting the road's superelevation.

At this point, it should be noted that the results will yield noisy values due primarily to accidental errors by the MLS and the noise added by the parameterisation process itself. A smoothing filter is applied to the diagrams to reduce these errors, and consists of locally weighted scatterplot smoothing (LOWESS). The anti-aliasing filtering used is a locally weighted regression curve (Cleveland, 1979; Cleveland and Devlin, 1988) based on the local adjustment of polynomial models that are joined in a subsequent step. The observations' weights in the adjustment are modified by accounting for their distance from the model (Eq. (8)):

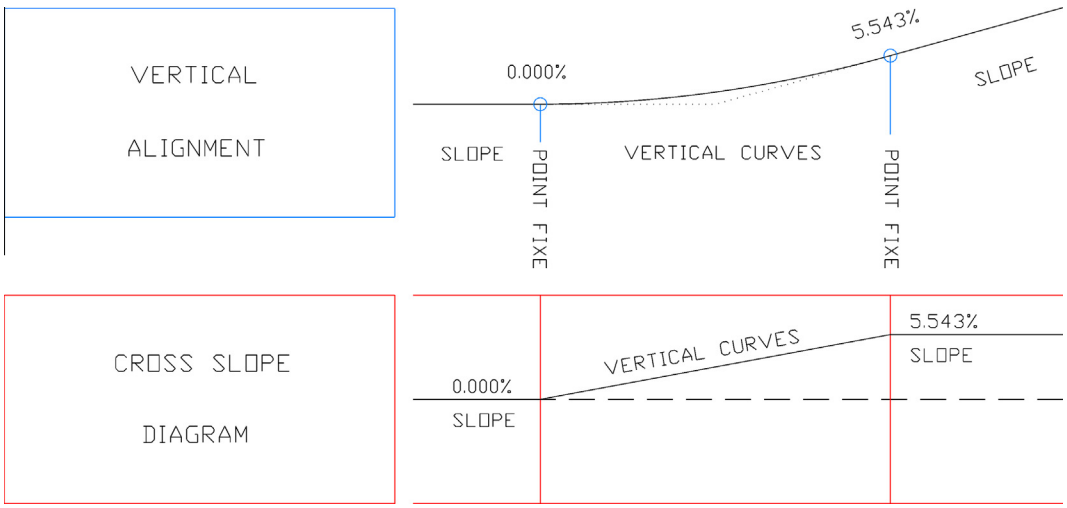

Fig. 6. Road parameterisation example taking into account the slope diagram. Road vertical alignment (top) and slope diagram parameterisation (bottom).

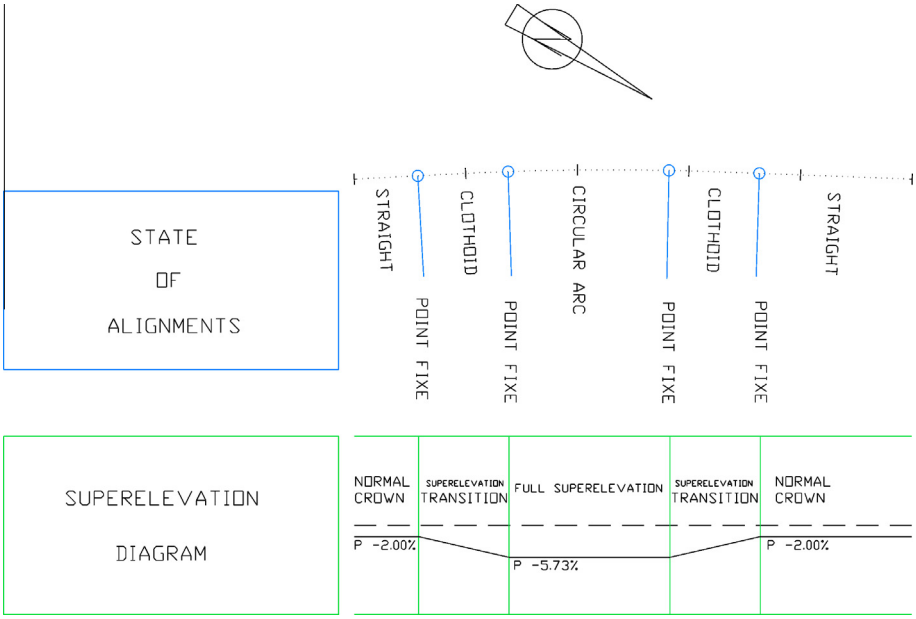

Fig. 7. Parameterisation of a road regarding cross-section slopes. Related floor plan of the road (top) and superelevation diagram (bottom) are shown in the diagram.

$$\omega_i = \left(1 - \left|\frac{x - x_i}{d(x)}\right|^3\right)^3 \tag{8}$$

where x is the predictor value associated with the response value to be smoothed, x_i are the nearest neighbours of x, and $d(x)$ is the distance along the abscissa from x to the most distant predictor value.

After applying the anti-aliasing filter to both the slope and superelevation values, the data are suitable for a classification in terms of the road's vertical geometric parameters.

Given that the road is segmented into equally spaced sections, the classification sections are distinguishable through histogram inspection. In fact, the histogram maxima correspond to a constant slope (slope diagram) as normal crown zones and full superelevation (superelevation diagram). Once the constant sections are classified, the joining sections must be modelled in both the slope and superelevation diagrams. These sections act as a connection of the constant zones in the diagrams and are modelled using least-square linear regression (Toutenburg, 2008) of the variable of interest using Eqs. (9)–(11):

$$y = \beta_1 + \beta_2 \cdot x + \varepsilon \tag{9}$$

$$y = \begin{bmatrix} p_1 \\ p_2 \\ \vdots \\ p_n \end{bmatrix} \quad x = \begin{bmatrix} 1 & s_1 \\ 1 & s_2 \\ \vdots & \vdots \\ 1 & s_n \end{bmatrix} \quad \beta = \begin{bmatrix} \beta_1 \\ \beta_2 \end{bmatrix} \quad \varepsilon = \begin{bmatrix} \varepsilon_1 \\ \varepsilon_2 \\ \vdots \\ \varepsilon_n \end{bmatrix} \tag{10}$$

$$\begin{bmatrix} p_1 \\ p_2 \\ \vdots \\ p_n \end{bmatrix} = \begin{bmatrix} 1 & s_1 \\ 1 & s_2 \\ \vdots & \vdots \\ 1 & s_n \end{bmatrix} \cdot \begin{bmatrix} \beta_1 \\ \beta_2 \end{bmatrix} + \begin{bmatrix} \varepsilon_1 \\ \varepsilon_2 \\ \vdots \\ \varepsilon_n \end{bmatrix} \tag{11}$$

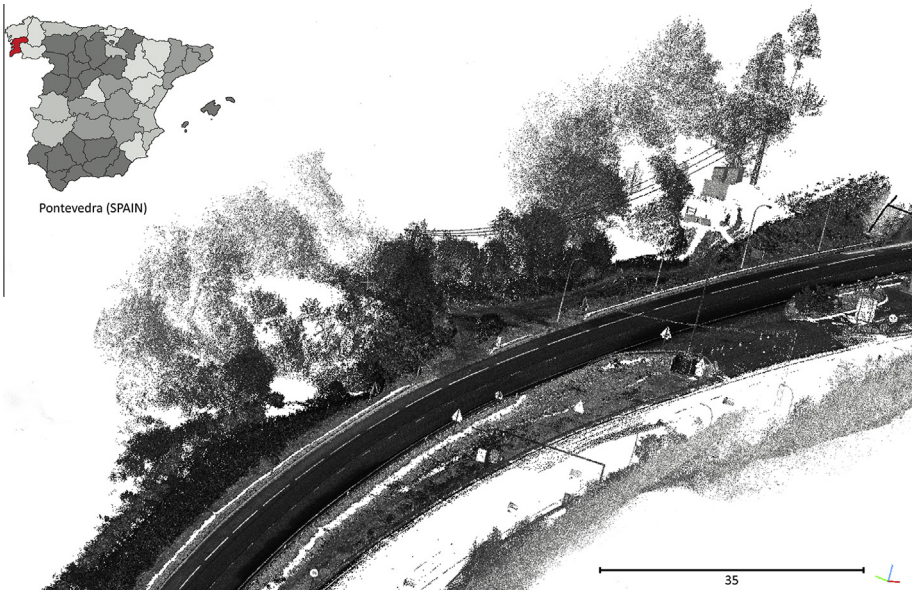

Fig. 8. Raw point cloud captured by LYNX Mobile Mapper on A-52 highway, in NW Spain.

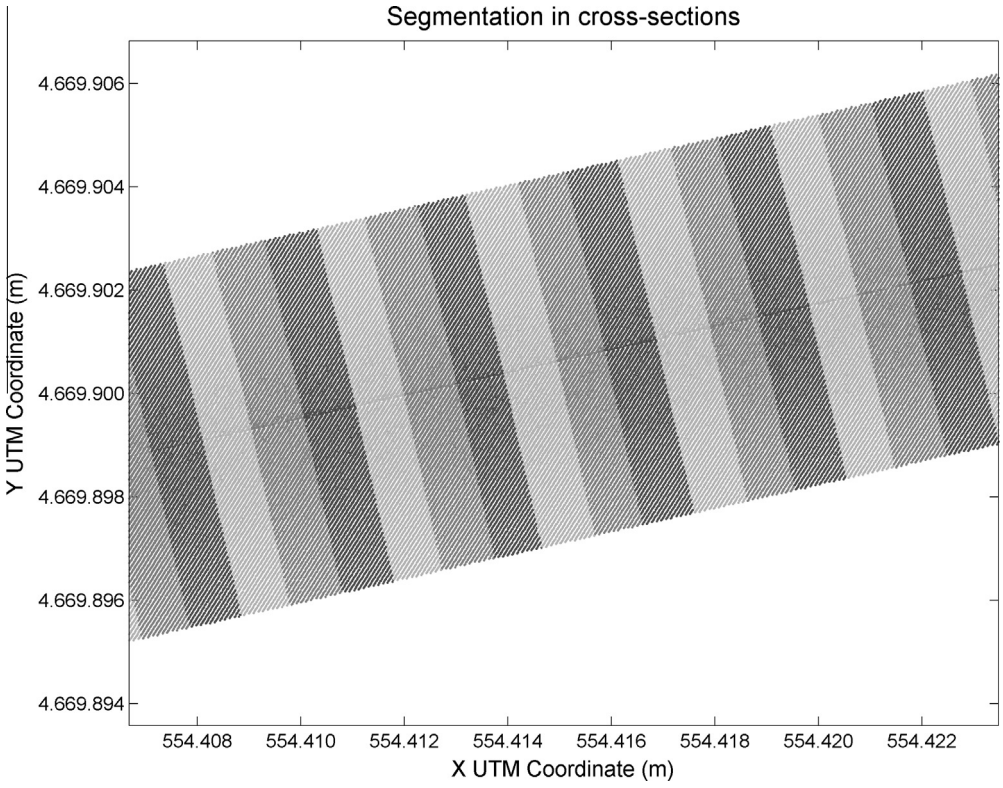

Fig. 9. Segmentation of the platform in cross-sections.

Table 2
Segmentation summary.

Segmentation	Points	Percentage (%)
Raw point cloud	97,214,162	100
Road platform point cloud	33,054,744	34
Cross-section (3747) points	8820	0.009

where p is the variable of interest (slope or superelevation, respectively), s is the distance between points, β_1 and β_2 are the parameters of the line and ε are the errors of the points.

When the diagrams are classified through histogram processing and linear adjustment, point fixes are extracted from the intersection of these lines and the horizontal lines in the diagram. Point fixes are the points where constant horizontal lines and transition straight lines meet (Figs. 6, 7 and 11). Other geometric characteristics of the road, such as section lengths, percentage slope and slope variation, can be calculated using these point fixes.

The sections and parameters obtained from this process are suitable for storage in a database that complies with the Spanish Official Road Rules regarding a road's route and geometric characteristics.

3. Experimental results

To test the developed methodology, a dataset is captured from the Spanish highway A-52 between marker posts 278/500 and 282/250. The point cloud obtained by the system is captured with a scanning frequency of 500,000 points per second and generated 97.2 million data points (Fig. 8).

Given the massive amount of input data, a segmentation is performed using angular thresholds and PCA-based adjustment, as described in the previous section (Fig. 2).

As a result, two angle thresholds between 196° and 336° are set. These values permit the road platform to be segmented, for a total of 33 million points. This segmentation is performed for the entire dataset because the case study consists of a highway where the superelevation is equal in all of the lanes.

Finally, the second segmentation provides 1 m spaced cross-sections along the MLS trajectory. These profiles are obtained based on the trajectory of the vehicle, as detailed in Section 2.3. 3747 Cross-sections are obtained in the case study and are 7 m wide, corresponding to the width of the platform. Each of the resulting rectangular areas comprises approximately 8800 points (Fig. 9).

As a summary of the segmentation process, Table 2 shows the number of points used for calculation and the reduction in the numbers of points needing processing in a row.

After segmentation is finished, a PCA-based adjustment is performed, supported by points belonging to the cross-sections. A sequence of planes along the trajectory is obtained as a result, which are processed to estimate the road slope and superelevation. As explained in Section 2.4, we perform the estimation using the covariance method. By using the covariance matrix's three eigenvalues and their corresponding eigenvectors, a vertical road alignment is computed for each of the 3747 cross-sections, and this is the number of vector sets defining the slope (v1) and the superelevation (v2) (Fig. 5). These vectors are used to compute a percentage parameter value.

Once the calculations of both the slope and superelevation are completed, we differentiate the geometric elements, as explained in Section 2.5. First, we obtain graphical diagrams for both the slope and superelevation (Fig. 10). Further analysis permits the sections in the diagrams to be differentiated and the data smoothing to be performed through LOWESS.

The different geometric elements are classified based on these graphical diagrams. The geometric parameters of interest are constant slopes and vertical curves (slope diagram) and normal crown zones and superelevation transitions and full superelevation

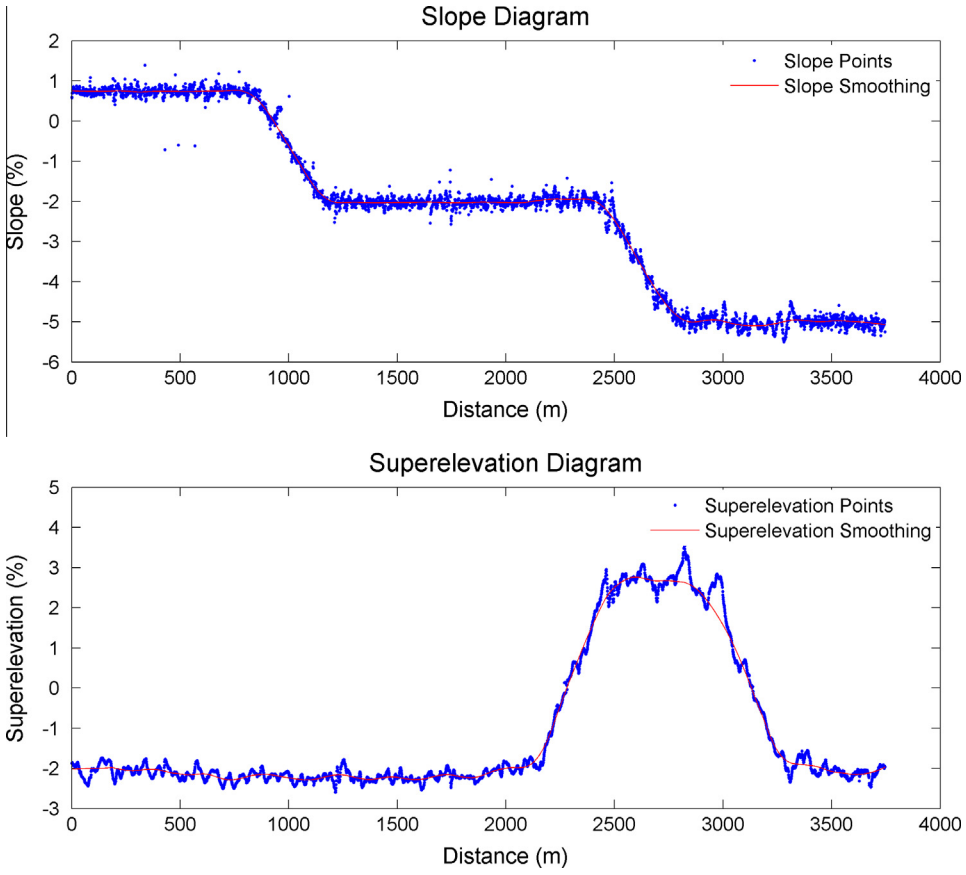

Fig. 10. Slope diagram (top) and superelevation diagram (bottom).

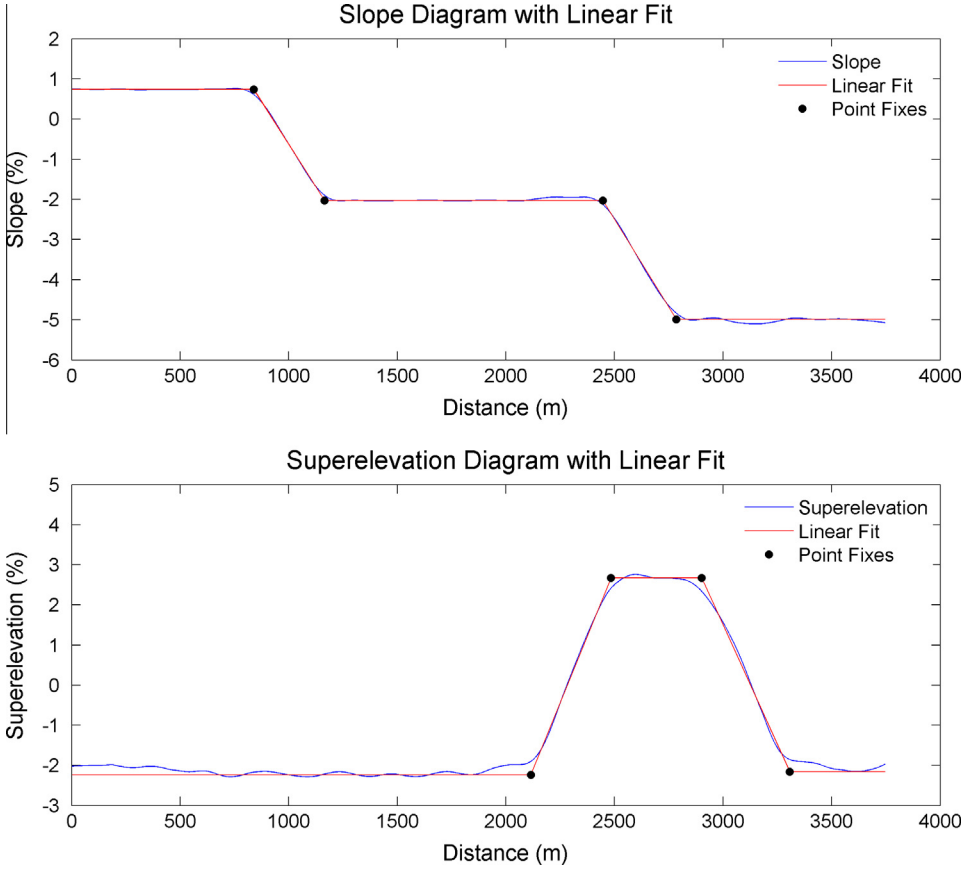

Fig. 11. Graphical diagrams after classification and linear adjustment of geometric elements and fixed points of: slope diagram and (top) superelevation diagram (bottom).

Table 3
Results compared to official data for geometric slope parameters.

Ground truth values		Calculated values (PCA)		Differences			Error (%)		
Length (m)	Slope (%)	Length (m)	Slope (%)	PK's	Slope	Length	PK's	Slope	Length
Slope extraction from A-52 highway									
0.000	0.717	0.000	0.741	0.000	−0.024	4.775	0.000	3.287	−0.566
843.049	0.717	838.274	0.741	4.775	−0.024	−4.396	−0.566	3.287	1.364
1165.458	−2.083	1165.080	−2.029	0.379	−0.054	0.252	−0.032	−2.572	−0.020
2447.267	−2.083	2446.636	−2.029	0.630	−0.054	−3.629	−0.026	−2.572	1.086
2781.375	−5.083	2784.374	−4.989	−2.999	−0.094	2.999	0.108	−1.841	−0.311
3746.028	−5.083	3746.028	−4.989	0.000	−0.094	–	0.000	−1.841	–

Table 4
Results compared to official data for geometric superelevation parameters.

Ground truth values		Calculated values (PCA)		Differences			Error (%)		
Length (m)	Super-elevation (%)	Length (m)	Super-elevation (%)	PK's	Super-elevation	Length	PK's	Super-elevation	Length
Superelevation extraction on A-52 highway									
0.000	−2.292	0.000	−2.238	0.000	−0.054	−1.138	0.000	−2.340	0.054
2113.139	−2.292	2114.277	−2.238	−1.138	−0.054	1.493	0.054	−2.340	−0.403
2483.902	2.768	2483.547	2.672	0.355	0.096	−0.263	−0.014	−3.482	0.063
2901.997	2.768	2901.905	2.672	0.092	0.096	−2.186	−0.003	−3.482	0.543
3304.788	−2.132	3306.881	−2.158	−2.093	0.026	2.093	0.063	1.238	−0.474
3746.028	−2.132	3746.028	−2.158	0.000	0.026	–	0.000	1.238	–

(superelevation diagram). The constant values (slope, normal crown and full superelevation) are obtained from the histogram of alignment, in which the maximum values correspond to these elements. Once the values are classified based on the histograms, we can determine inflection points by the intersection of constant values with linear fit slopes and superelevations belonging to the vertical curves and superelevation transitions, respectively (Fig. 11).

The results of the obtained slope's geometric elements are shown in Table 3, while the geometric elements of the superelevation are shown in Table 4. In both cases, the results are compared to the ground truth values provided by the Spanish Ministry of Development.

Analysing the data in Table 3, we can see the differences in both quantitative value and percentage, resulting in a maximum length difference of 4.775 m for the first slope and a maximum slope difference of −0.094%. The mean difference in the slope results is −0.06%. Regarding the relative errors in percentage, the biggest obtained mistake is 3.3%, while the average percentage relative error was −0.38%. These error values show that the developed methodology offers satisfactory results.

Analysing the data in Table 4, we can see a differences in both quantitative value and percentage. The maximum length difference is −2.186 m for the second superelevation transition, a percentage of 0.096%. The mean difference in the superelevation values is 0.03%. In terms of the relative errors, we obtain a maximum value of 3.482%, while the average percentage relative error for superelevation is −1.53%. In conclusion, the superelevation of the road calculated with the proposed methodology yields satisfactory results.

Overall, in both conducted analyses, the results extracted for slopes and are very similar, where the absolute length differences for linear elements become greater as the sections increase. On the contrary, the differences in superelevation become smaller as the methodology operates in a smaller range. The percentage relative errors are higher for angular measurements than for linear measurements in terms of both slope and superelevation. Noting the absolute differences in slope and superelevation, we can see that the results are below 0.1%, which is the maximum error considered in the inventory of Spanish roads.

4. Concluding remarks

This paper presented a contribution to data processing tasks for MLS. The developed methodology for road characterisation is based on segmentation processes, orthogonal regression through PCA and filtering. These procedures permit the determination of geometric parameters that best define vertical road alignments, such as slope, vertical curves, normal crown, full superelevation and superelevation transitions. The extracted geometric parameters comply with the Spanish normative.

In short, this paper's novel contribution is to propose an alternative for the automated development of "as-built" road plans. Based on the results, users can perform various analyses of interest about road conditions to determine constructive errors and prevent accidents.

The experimental results validate the use of the proposed method, guaranteeing relative accuracies under 3.5%. However, it should be noted that the proposed approach is a first approximation tested only for simple regional roads. It is not within the scope of this paper to provide a universal or commercial solution for any type of road.

Accounting for the results and comparing them with existing research (Lakakis et al., 2013; Tsai et al., 2013), the present study provides comprehensive information on vertical alignments, both longitudinally and transversely and for both lanes of a road. The methodology presented in this article goes a step further in the extraction of information. An input LiDAR point cloud enables for the precise analysis of road conditions and does not rely on the trajectory followed by the driver.

Despite the large volume of information generated by this type of system, the developed methodology obtains detailed information easily and smoothly due to the simple algorithms implemented. The automatic extraction of road elevations and cross-sections in an accurate manner will be important to further studies on road visibility.

In the future, the georeferenced information captured by the MLS, horizontal alignment and vertical alignment could be used for visibility studies and serve as a complete tool for road maintenance and quality control.

Acknowledgements

The authors would like to thank the Ministerio Ciencia e Innovación (Grant No. IPT-2012-1092-120000; INNPACTO program) for the financial support given. Furthermore, a portion of human resources for this work has been supported by the European Regional Development Fund (FEDER), the Spanish Centre for Technological and Industrial Development (Grant No. IDI-20101770) and Xunta de Galicia (Competitive Referenced Research Groups, Grant No. 2012/269) (Human Resources programs BES-2010-034106 and IPP055 – EXP44).

References

Ai, C., Tsai, Y.J., 2012. Critical assessment of automatic traffic sign detection using three-dimensional LiDAR point cloud data. In: Transportation Research Board 91st Annual Meeting, pp. 12–3214.

Belton, D., Lichti, D.D., 2006. Classification and Segmentation of Terrestrial Laser Scanner Point Clouds using Local Variance Information. IAPRS, XXXVI, 5.

Cleveland, W.S., 1979. Robust locally weighted regression and smoothing scatterplots. J. Am. Stat. Assoc. 74 (368), 829–836.

Cleveland, W.S., Devlin, S.J., 1988. Locally weighted regression: an approach to regression analysis by local fitting. J. Am. Stat. Assoc. 83 (403), 596–610.

Di Mascio, P., Di Vito, M., Loprencipe, G., Ragnoli, A., 2012. Procedure to determine the geometry of road alignment using GPS data. Procedia-Soc. Behav. Sci. 53, 1203–1216.

El-Halawany, S.I., Lichti, D.D., 2011. Detection of road poles from mobile terrestrial laser scanner point cloud. In: Multi-Platform/Multi-Sensor Remote Sensing and Mapping (M2RSM), 2011 International Workshop on, pp. 1–6.

Gikas, V., Stratakos, J., 2012. A novel geodetic engineering method for accurate and automated road/railway centreline geometry extraction based on the bearing diagram and fractal behavior. IEEE Trans. Intell. Transp. Syst. 13 (1), 115–126.

Gomes, S.V., 2013. The influence of the infrastructure characteristics in urban road accidents occurrence. Accid. Anal. Prevent 60, 289–297.

Gräfe, G., 2008. Kinematic 3D laser scanning for road or railway construction surveys. In: Proceedings of the International Conference on Machine Control & Guidance, pp. 24–26.

Holgado-Barco, A., González-Aguilera, D., Arias-Sanchez, P., Martinez-Sanchez, J., 2014. Semi-Automatic extraction of road horizontal alignment from a mobile LiDAR system. Comput.-Aided Civil Inf. Eng. http://dx.doi.org/10.1111/mice.12087.

Institute for Road Safety Research, 2002. Safety Standards for Road Design and Redesign SAFESTAR, pp. 1–118.

Jolliffe, I.T., 2002. Principal Component Analysis, second ed. New York, Springer.

Karamanou, A., Papazissi, K., Paradissis, D., Psarianos, B., 2010. Precise Estimation of Road Horizontal and Vertical Geometric Features using Mobile Mapping Techniques. Boletim De Ciências Geodésicas, 15(5).

Lakakis, K., Savvaidis, P., Wunderlich, T., 2013. Evaluation of a low-cost mobile mapping and inspection system for road safety classification. Am. J. Geogr. Inf. Syst. 2 (1), 6–14.

Optech Inc., 2013. Home page of The Company Optech Inc. <http://optech.ca> (3.12.2013).

Pauly, M., Gross, M., Kobbelt, L.P., 2002, October. Efficient simplification of point-sampled surfaces. In: Proceedings of the Conference on Visualization'02, IEEE Computer Society, pp. 163–170.

Puente, I., González-Jorge, H., Riveiro, B., Arias, P., 2012. Accuracy verification of the LYNX mobile mapper system. Opt. Laser Technol.

Sentouh, C., Glaser, S., Mammar, S., 2006. Advanced vehicle–infrastructure–driver speed profile for road departure accident prevention. Vehicle Syst. Dyn. 44 (sup1), 612–623.

Taylor, D.R., Muthiah, S., Kulakowski, B.T., Mahoney, K.M., Porter, R.J., 2007. Artificial neural network speed profile model for construction work zones on high-speed highways. J. Transport. Eng. 133 (3), 198–204.

Toutenburg, H., 2008. Linear Models and Generalizations: Least Squares and Alternatives. Springer.

Tsai, Y.J., Ai, C., Wang, Z., Pitts, E., 2013. A mobile cross slope measurement method using LiDAR technology 2. Technology 2 (3), 4.

Wang, J., González-Jorge, H., Lindenbergh, R., Arias-Sánchez, P., Menenti, M., 2013. Automatic estimation of excavation volume from laser mobile mapping data for mountain road widening. Remote Sens. 5 (9), 4629–4651.

Yang, B., Fang, L., Li, Q., Li, J., 2012. Automated extraction of road markings from mobile LiDAR point clouds. Photogramm. Eng. Remote Sens. 78 (4), 331–338.